Water Resources Research

RESEARCH ARTICLE
10.1029/2018WR024217

Spanwise Cylinder Wake Hydrodynamics and Fish Behavior

V. Muhawenimana[1], C. A. M. E. Wilson[1], P. Ouro[1], and J. Cable[2]

[1]School of Engineering, Cardiff University, Cardiff, UK, [2]School of Biosciences, Cardiff University, Cardiff, UK

Key Points:
- The interaction of fish with spanwise vortices was examined by considering habitat use and swimming stability
- Fish avoided areas of highest turbulent heterogeneity, while loss of stability peaked when turbulence length scale was 45–50% of fish length
- Highest magnitudes of downward-acting Reynolds stresses and negative vorticity corresponded to the highest rate of spill occurrence

Supporting Information:
- Supporting Information S1

Correspondence to:
V. Muhawenimana,
MuhawenimanaV@cardiff.ac.uk

Citation:
Muhawenimana, V., Wilson, C. A. M. E., Ouro, P., & Cable, J. (2019). Spanwise cylinder wake hydrodynamics and fish behavior. *Water Resources Research*, *55*, 8569–8582. https://doi.org/10.1029/2018WR024217

Received 5 OCT 2018
Accepted 10 OCT 2019
Accepted article online 24 OCT 2019
Published online 6 NOV 2019

Abstract Flows generated near hydro-engineering structures are characterized by energetic three-dimensional flow structures that are markedly different from naturally occurring fish habitats. The current study evaluated the interaction of Nile tilapia (*Oreochromis niloticus*) with spanwise rollers in the turbulent wake of a cylinder in both the wake bubble and the vortex shedding further downstream. The flow field hydrodynamics were measured using an acoustic Doppler velocimeter for Reynolds number (Re_D) regimes ranging from 3,730 to 33,590, over a streamwise length of six diameters downstream of the cylinder, and revealed a pair of alternating vortices rotating about a spanwise axis, which were rendered asymmetric by the bed boundary proximity. Fish avoided areas where vorticity, turbulence intensity, turbulent kinetic energy, eddy size, and Reynolds shear stress were highest. Events of stability loss, referred to as spills, were significantly correlated to the turbulence integral length scale relative to fish standard length, with the peak number of spills occurring when the eddy length approached 45% to 50% of the fish length. Spill events significantly depended on Re_D, Reynolds stress, and vorticity and varied according to fish length and weight. Among zones of similar Reynolds stress and vorticity magnitude, spills were most frequent when Reynolds shear stress was positive, downward acting and eddies rotated clockwise, which highlights the importance of direction and orientation of flow structures in determining the hydrodynamic forces that affect fish swimming stability. Recommendations are made for the inclusion of these metrics in the design and refinement of hydro-engineering schemes.

1. Introduction

Modifications to river habitats through hydraulic structures have significantly affected aquatic species by creating unnatural flows. Fragmentation of riverine habitats is particularly problematic for fish species, disrupting short- and long-distance migrations (Fuller et al., 2015; Katopodis & Williams, 2012) and creating extreme conditions that may impact fish habitat preferences, feeding, spawning, swimming ability, and swimming kinematics (Hockley et al., 2014; Murchie et al., 2008; Williams et al., 2012). River restoration schemes attempt to restore the aquatic environment back to natural conditions, and fish passes facilitate movement of migratory species with varying efficiency (Larinier, 2001; Noonan et al., 2012). Such restorations, however, only achieve seminatural conditions and often create a wider range of flow heterogeneity in terms of velocities, turbulence, and turbulent shear stresses, particularly problematic for smaller or weaker swimmers (Lacey et al., 2012; Silva et al., 2011; Wang et al., 2010, 2016).

Both field and laboratory studies indicate that altered and turbulent flows can be both beneficial and detrimental to fish (Enders et al., 2003; Liao, 2007; Pavlov et al., 2000; Tritico & Cotel, 2010; Webb, 1998) affecting their swimming behavior, aggregation, and migration (Lacey et al., 2012; Liao, 2007; Pavlov et al., 2000). Fish can take advantage of turbulent flows to reduce energy expenditure (Enders et al., 2003; Liao et al., 2003; Webb, 1998). Fish also choose low momentum paths available in the wake of an object and synchronize their swimming trajectory by "Karman gaiting" between von Kármán-type alternating vortex shedding, therefore exploiting the rotating motion of these rollers to propel themselves upstream (Liao et al., 2003). Fish use their lateral line to sense the velocity and pressure field properties in their environment, as well as vortices generated by the movement of other fish and those in the wake of an obstruction. Conversely, negative effects of turbulence on fish swimming ability manifest as highly turbulent flows create swimming instabilities, increase energy expenditure, and decrease swimming performance (Pavlov et al., 2000; Nikora et al. 2003; Lupandin, 2005; Cotel et al., 2006; Liao et al., 2003; Webb, 1998; Enders et al., 2003; Plew et al., 2007; Tritico & Cotel, 2010; Maia et al., 2015; Wang & Chanson, 2018). The conflicting findings of whether turbulence and large-scale vortices are beneficial or detrimental might be explained by the different intensity,

periodicity, orientation, and scale characteristics of the turbulent flows, which have varied across studies (Lacey et al., 2012; Murchie et al., 2008).

Losses in swimming stability in response to perturbations are important to evaluate because fish expend energy and time recovering from instabilities while navigating challenging flows at the cost of swimming speed, effects that vary depending on flow velocity, turbulence vorticity characteristics, and fish length (Cada & Odeh, 2001; Lupandin, 2005; Maia et al., 2015; Pavlov et al., 2000; Tritico & Cotel, 2010), as well as turbulence intensity and shear stresses (Cotel et al., 2006; Silva et al., 2011). Tritico and Cotel (2010) identified a relationship between turbulence eddy diameter and fish body length, where eddies over 75% of fish length destabilized the fish, confirming previous investigations into the effects of turbulence on the swimming ability of fish (Cada & Odeh, 2001; Liao, 2007; Pavlov et al., 2000). This ratio of turbulent length scale to fish length that destabilize the fish has also been identified as 66% (Lupandin, 2005) and in the range of 50% to 100% (Webb & Cotel, 2011). Vertical rollers are shed from vertically orientated objects, spanwise rollers are shed from objects with axes that span the cross-flow direction, and streamwise rollers have axes of rotation parallel to the flow direction; all incite different adverse responses from fish (Maia et al., 2015; Tritico & Cotel, 2010). Indeed, the orientation of flow obstructions and the axis of rotation of their wake eddies are vital since spanwise rollers have a greater impact on swimming stability and critical swimming speed than vertical rollers by requiring more recovery maneuvers from the fish (Tritico & Cotel, 2010).

Cylindrical-shaped objects, often used in hydrodynamic research, are abundant in fluvial environments, including vegetation, woody debris, pipes, or bridge piers. They generate coherent and periodic turbulent flow structures against which fish swimming behavior can be studied. Recent research focus on flow around horizontal cylinders has shown that these can exhibit different vortex shedding regimes compared to vertical cylinders (Lehmkuhl et al., 2013). In addition to the Reynolds number, the characteristics of the unsteady wake behind a horizontal cylinder depends on its proximity to the solid boundary and the approaching boundary layer thickness that affects the cylinder hydrodynamic and lift forces, the location of frontal stagnation points and shear separation layers, the extent of the recirculation bubble, and symmetry of the von Kármán street (Oner et al., 2008; Price et al., 2002; Sarkar & Sarkar, 2010).

Our understanding of the threshold of hydrodynamic conditions that lead to disruption of fish swimming kinematics is incomplete. Therefore, to further investigate the swimming stability and habitat usage of fish in altered turbulent flows, the current study tested fish swimming kinematics in the wake of a horizontal cylinder model. The cylinder wake's hydrodynamic properties were measured, and fish of various lengths were tested under a wider range of cylinder Reynolds numbers.

2. Materials and Methods

2.1. Flume Setup and Test Area

Experiments were performed in an open channel recirculating Armfield flume with glass walls (1,000-cm length, 30-cm width, and 30-cm height) in the Cardiff School of Engineering Hydro-environmental Research Centre laboratory. The flume was set to a slope of 1/1000. An electromagnetic flowmeter (Euromag MUT1100) measured the water discharge (±0.3% L/s). A cylinder, 5-cm diameter (D), was placed transversally across the flume width and fixed to the flume walls using silicon adhesive, with its center 5 cm from the flume bed. The ratio of the gap distance between the cylinder and the flume bed (G) relative to the cylinder diameter (G/D) was 0.5 and corresponding to a vertical distance whereby the proximity to the bed affects the vortex shedding mechanisms while not too confined to suppress the shedding phenomenon (Oner et al., 2008). Flow over and under the cylinder generated a turbulent wake that was used to test the fish swimming kinematics. Honeycomb flow diffusers bounded the test section, 5-cm upstream and 30-cm downstream of the cylinder, with the upstream flow diffuser located 380 cm from the upstream end of the flume (Figure 1). A streamwise-averaged flow depth (H) of 15 cm, measured using a Vernier pointer gauge (±0.1 mm) along the flume centerline, was maintained for all tests using a tailgate weir located downstream of the flume, resulting in cross-sectional averaged velocities and Reynolds numbers shown in Table 1. The local flow depth (H_L) was measured in streamwise increments of 5 cm to characterize the effects of the cylinder and shallowness of the flow, on the surface water profile. Flow discharges (Q) ranged from 3 to 27 L/s and cross-sectional averaged velocities ranged from 6.67 to 60 cm/s (Table 1). The wake of the cylinder was within Re_D ranges of the subcritical regimes and was fully turbulent (Douglas et al., 2011). A Logitech HD

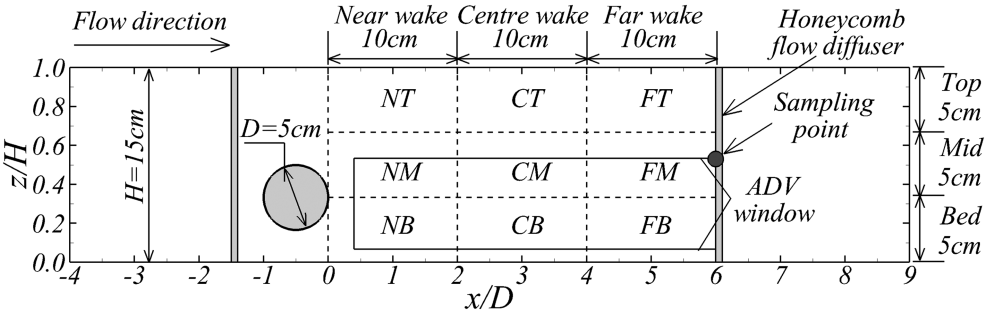

Figure 1. Side view of the fish behavior observation test section, located 3.8-m downstream of the flume inlet and subdivided into flow volume zones of equal demensions, with length of 10 and 5 cm in the streamwise (x) and vertical (z) directions, respectively. The origin of the x axis corresponds to the edge of the cylinder and the flume bed for the z axis. Flow volume zones are named as follows: NB for the near wake bed, NM for the near wake midwater column, and NT for the near wake top water column. Similary, CB, CM, CT, FB, FM, and FT refer to the bed-water, midwater, and top-water column zones in the center and far wakes of the cylinder. The spectral analysis sampling point located at $x/D = 6$, $z/H = 0.53$ is shown.

web camera, C920, with a 720p–1080p resolution at 30 frames per second positioned on the glass side of the flume recorded a side elevation view of the fish swimming behavior.

2.2. Fish Swimming Behavior Tests

Nile tilapia (*Oreochromis niloticus*, Silver strain; $n = 28$; fork length [11.78 ± 2.11 cm]; standard length, herein referred to as L_{fish} [9.52 ± 1.77 cm] and weight [31.6 ± 17.5 g]) sourced from a commercial facility (FishGen Ltd.), were maintained in aquaria facility in the Cardiff School of Biosciences at 25 ± 0.5°C. This temperature was also maintained during acclimatization of the fish in the flume and for all swimming tests. Individual swimming tests were conducted using a ramped step velocity test after each fish was acclimatized in an area downstream of the test section in the flume for 30 min, at the lowest discharge of 1.5 L/s. The acclimatization space was also delimited by honeycomb flow diffusers, which were lifted to allow fish to swim in the test section at the beginning of the velocity step test and behavior observations. Discharges were increased from 3 to 27 L/s in step increments of 3 L/s, and each velocity step was maintained for a test time of 10 min during which fish swimming kinematics were observed. Fish maintenance and behavioral tests were all approved by Cardiff University Animal Ethics Committee and conducted under Home Office license PPL 303424.

Videos of the swimming behavior were reviewed, and habitat preference as well as swimming behaviours were logged using JWatcher V1.0 software to record the amount of time fish spent in each flow volume of the test section, the time or velocity step and the volume zone where spills occurred. The body center was used to locate the fish. Flow volume zones were defined by dividing the test section into nine subsections of equal dimensions. Three sections (10-cm length) along the streamwise direction delimited the near, center, and far wakes, while three sections (5-cm height) in the vertical direction delimited the water column into bed-water, midwater, and top-water column volume zones (see Figure 1). Spills, events of loss of balance, were defined by Tritico and Cotel (2010) as involuntary swimming behavior where the fish's head rotates more than 45° in yawing motion, followed by drifting downstream over a distance longer than half of its body length. Recovery maneuvers from the spill follow as the fish realigns its body length to the longitudinal flow direction. A measure of the rate of spill occurrence used in this study was the ratio of the number of spills over the amount of time spent in each flow volume, referred to as spill frequency (min^{-1}).

2.3. ADV Velocity Data Acquisition

The hydrodynamic characteristics of the cylinder wake were measured using an acoustic Doppler velocimeter (ADV), a downward-looking Nortek Vectrino Plus (V.1.31+) at a sampling rate of 200 Hz. The flow was seeded with neutrally buoyant sphericel hallow glass silicate powder with 10-μm mean diameter and 1.1 ± 0.05 g/cm^3 density (Potters Industries Inc.). The sound-to-noise ratio and correlation were maintained above 20 dB and 70%, respectively, by adding the seeding material to the water to ensure good quality data. Recorded velocities were in three dimensions of xyz coordinates, x longitudinal, y transverse, and z vertical

Table 1
Details of the velocity step test used for fish swimming behavior with time increments (each 600 s) and flow rate (Q) with corresponding cross-sectional averaged velocity (U_0), Froude number (Fr), and cylinder Reynolds number (Re_D), vortex shedding peak frequency (f), and Strouhal number (St) at 25°C

Time (min)	Q (L/s)	U_0 (cm/s)	Fr	Re_D	f (s^{-1})	St (–)
0–10	3	06.67	0.05	3,730	0.46	0.34
10–20	6	13.33	0.11	7,470	0.85	0.32
20–30	9	20.00	0.16	11,200	1.21	0.30
30–40	12	26.67	0.22	14,930	1.61	0.30
40–50	15	33.33	0.27	18,660	2.00	0.30
50–60	18	40.00	0.33	22,400	2.62	0.32
60–70	21	46.67	0.38	26,130	3.04	0.32
70–80	24	53.33	0.44	29,860	3.05	0.28
80–90	27	60.00	0.49	33,590	4.05	0.33

flow directions. The spatial resolution of the velocity sampling grid was such that along the flume centerline, 15 points were measured equispaced by 2 cm in the x direction and 15 points, 0.5 cm apart in the z direction. A constant sampling time of 300 s was used for all data points. The geometry of the ADV probe did not permit velocity measurements within 2.5-cm distance from the edge of the cylinder and in a distance greater than 8 cm from the flume bed, which meant that parts of the midwater column and top layer of the water column (see Figure 1) were not included in the velocity measurements. The accuracy of an ADV probe has been compared to other velocity probes (e.g., pitot tube) and found to be within 2%, based on integrating the velocity measurements over the water column (Leng & Chanson, 2017).

2.4. ADV Data Filtering and Postprocessing

The Velocity Signal Analyzer (MAJVSA version V1.5.62) was used to filter and despike the ADV data using limits of 15 dB and 70% for sound-to-noise ratio and correlation, respectively (Nortek, 2009). Further despiking used the phase–space thresholding method by Goring and Nikora (2002; revised by Wahl, 2003) as well as a 12-point average spike replacement (Jesson et al., 2013). On average, the percentage of good samples after filtering and despiking was 80%. Turbulence characteristics calculated using MAJVSA included the turbulent kinetic energy ($TKE = 0.5\left(\overline{u'^2} + \overline{v'^2} + \overline{w'^2}\right)$, longitudinal turbulence intensity $\left(TI_u = \sqrt{\overline{u'^2}}\right)$, and Reynolds shear stresses $\left(\tau_{uv} = -\rho\left(\overline{u'v'}\right)\right)$,and $(\tau_{uw} = -\rho\left(\overline{u'w'}\right))$ for the spanwise and vertical components, respectively. Note that overbar $(\bar{\cdot})$ denotes time averaging.

A FORTRAN script was used to perform the autocorrelation function integration and calculation of the turbulence length scale (Pope, 2000). The autocorrelation function $\varphi(t)$ is

$$\varphi(t) = \frac{\overline{u'(t)\cdot u'(t+s)}}{\overline{u'(t)^2}}, \tag{1}$$

where s is the lag time and u′ denotes velocity fluctuation values. The longitudinal turbulent integral length scale L_u is given by

$$L_u = \overline{u}\int_0^T \varphi(t)dt, \tag{2}$$

where T is the time at which the autocorrelation function becomes firstly negative, that is, $\varphi(T) = 0$, and $\overline{u}$ is the mean streamwise velocity at the evaluated point. The 2-D vorticity field definition based on the time-averaged velocity gradient about a given axis is used in this study (see Crowder & Diplas, 2002; Graf & Yulistiyanto, 1998; Jamieson et al., 2013). It assumes that for a time-averaged flow field, the mean velocity for a given point in space does not vary with time, and therefore, the associated time-averaged vorticity field must also be constant. The spanwise component, that is, in the direction of the cylinder's axis, of the mean vorticity vector based on the time-averaged streamwise $\overline{u}$ and vertical velocities $\overline{w}$ is given by

$$\omega_y = \frac{\Delta\overline{w}}{\Delta x} - \frac{\Delta\overline{u}}{\Delta z}, \tag{3}$$

where Δx and Δz are the distances between two consecutive measurement locations in the streamwise and vertical directions, respectively, and $\Delta\overline{u}$ and $\Delta\overline{w}$ are the variations of the velocity values between those locations. Note that this definition is used as the measurement points closest to the cylinder's lee-side are 2 cm downstream and that closest to the flume's bottom is at an elevation of 0.5 cm. Strouhal number is defined by

$$St = \frac{f\cdot D}{U_0}, \tag{4}$$

where f is the dominant shedding frequency identified from the high spectral energy peaks obtained from the fast Fourier transform (FFT), D is the cylinder diameter, and U_0 is the cross-sectional averaged velocity

(Pope, 2000). The recurrent generation of instantaneous turbulent structures were identified from the computed fast Fourier transform of the time series of all three velocity components u, v, and w at the sampling point $x = 6D$, $z = 0.53H$ in the cylinder wake.

2.5. Statistical Analysis

Fish behavior data in relation to hydrodynamic parameters were analyzed in R statistics software (3.5.0; R Core Team, 2018) via RStudio (Version 1.1.447; RStudio Team, 2016). Mean, standard deviation, and quartiles of each variable were summarized and Shapiro tests used to evaluate the data distributions. Generalized linear mixed models (GLMMs) using Fish ID to account for repeated measures of fish were used to evaluate the number of spills in each zone as explained by the fish characteristics (length and weight), the amount of time spent in each zone, the longitudinal and vertical distance of the zone where the spill occurred, the Reynolds number and flow velocity, and turbulence properties which are spatially averaged for each zone ($\langle\overline{u}\rangle$, $\langle\overline{v}\rangle$, $\langle\overline{w}\rangle$, $\langle\overline{u'}\rangle$, $\langle\overline{v'}\rangle$, $\langle\overline{w'}\rangle$, $\langle TKE\rangle$, $\langle\omega_y\rangle$, $\langle\boldsymbol{\tau}_{uv}\rangle$, $\langle\boldsymbol{\tau}_{uw}\rangle$, and L_u). Note the angle brackets $\langle\cdot\rangle$ denote spatial averaging. Similar GLMMs were used to evaluate the proportion of time and the frequency of spills in each flow volume zones for each fish. The GLMM models used Lmer and Lme4 R packages (Bates et al., 2015) and were refined by minimizing the Akaike information criterion.

3. Results

3.1. Turbulent Wake Dynamics

Swimming stability and microhabitat use of Nile tilapia was studied in the wake of a horizontal cylinder in a step velocity test with nine Reynolds numbers ranging from $3{,}730 \leq Re_D \leq 33{,}590$. Under these conditions, the cylinder flow is within the subcritical regime in which the laminar shear layer breakdown off the walls of the cylinder generated coherent alternating von Kármán vortex shedding with vortices with spanwise axes of rotation (Williamson, 1996). As the flow accelerated over and under the cylinder, clockwise and counterclockwise rotating vortices formed off the upper and lower cylinder walls, respectively.

Due to the presence of the cylinder and flow shallowness, surface standing waves were generated immediately downstream of the cylinder and were contained within a region of londitudinal distance 6D, throughout the test section (Figure 1), while the upstream flow depth remained constant and was only slightly elevated at higher Reynolds numbers (see Figure 2). The presence of surface waves resulted in a nonhydrostatic pressure field in the test section.

The normalized time-averaged hydrodynamics developed in the cylinder wake were similar for all Reynolds numbers, and Figure 3 presents those corresponding to the $Re_D = 16{,}800$ case. A wake bubble was generated immediately downstream of the cylinder, as depicted from the contours of $\overline{u}$ in Figure 3a, which reduced in streamwise extent with increasing Reynolds number (data not shown). The impact of the small gap between the cylinder and flume bed induced large vertical velocities $\overline{w}$ and turbulence intensities which, in turn, contributed to the asymmetric formation and shedding of the von Kármán type vortices in the cylinder wake. Indeed, across the range of Re_D tested, the gap between the cylinder and the bed resulted in mean flow hydrodynamics featuring asymmetric vorticity field with predominantly clockwise vortices over the wake length as indicated by the large area occupied by negative vorticity, which correlate well with the regions of highest Reynolds shear stress (Figures 3e and 3f). The large-scale vortical structures dissipated with increasing downstream distance from the cylinder such that the near wake ($x/D < 2$) showed higher magnitudes of longitudinal (Figure 3c), lateral and vertical turbulence intensities than the center and far wakes (see Figure 1 for notation).

At each discharge, spectral energy analysis showed that the frequency of the energy peaks related to the von Kármán type vortex shedding increased linearly with increasing Re_D with frequencies ranging from 0.46 to 4.05 s^{-1}, and corresponding Strouhal numbers remaining remarkably constant irrespective of Re_D with a mean value of 0.31 ± 0.02 (mean $\pm$ SD; Table 1). Note that these St values are higher than those for unbounded cylinder flows ($St = 0.21$) due to the proximity of the bed, in addition to the effects of free-surface dynamics. Such wake development is asymmetric as the vortices are constrained by the proximity of the bed and thus bottom vortices can only be horizontally propagated in the streamwise direction. This complex flow pattern of energetic turbulent structures spaned across the entire flume's width and occupied a large extent of the water column.

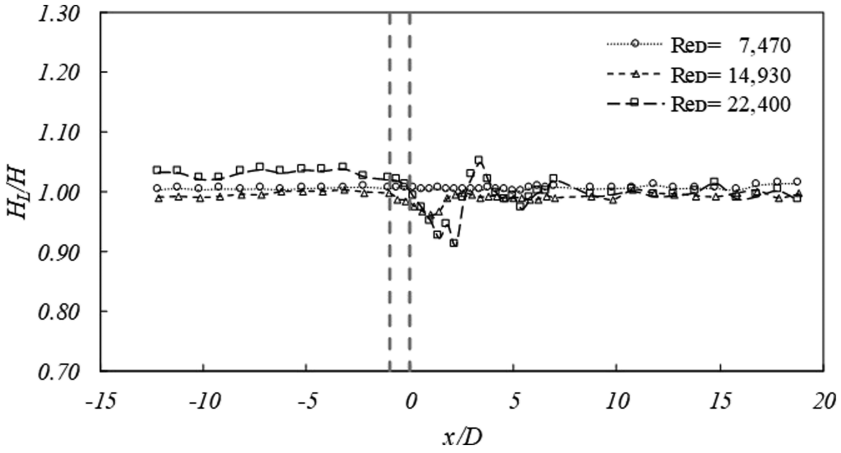

Figure 2. Longitudinal surface water profile as a function of the Reynolds number. The vertical dotted lines denote the cylinder edges, H is the streamwise-averaged flow depth and H_L is the local flow depth.

3.2. Fish behavior

3.2.1. Distribution of Habitat Usage Over the Step Velocity Test

Habitat usage (percentage of time) did not vary significantly with cylinder Reynolds number throughout the step velocity test (GLMM, d.f.1, $p > 0.05$) as the proportion of time fish spent in each flow volume zone (defined in Figure 1) remained uniform with increasing Re_D (Figure 4). Spatially, however, the percentage of time spent increased with increasing longitudinal distance from the cylinder (GLMM, d.f.1, $p < 0.001$) and decreased with increasing vertical distance, as fish stayed closer to the flume bed instead of swimming higher in the water column (GLMM, d.f.1, $p < 0.001$). Hence, the most preferred zone, far bed (FB), where fish spent 55% of time was furthest from the cylinder and closest to the flume bed (Figure 5a). Less than 2% of time was spent in each of the near wake zones, which are the most unstable regions with the highest magnitudes of turbulence intensity, turbulent kinetic energy, Reynolds shear stress, and vorticity, as shown

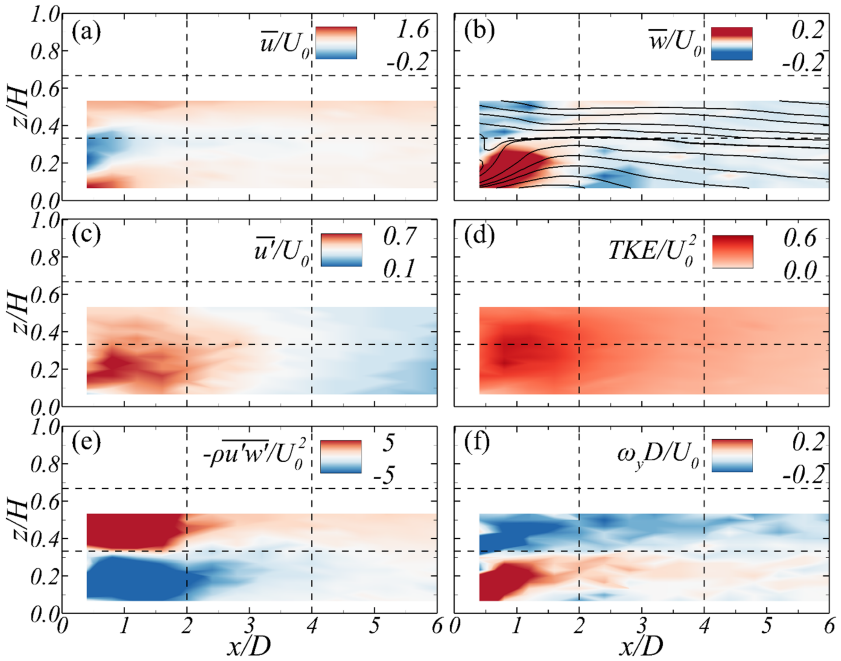

Figure 3. Time-averaged (a) streamwise velocity $\overline{u}$, (b) vertical velocity $\overline{w}$, (c) streamwise $\overline{u'}$ turbulence intensity, (d) turbulent kinetic energy TKE, (e) principal Reynolds shear stress–$\rho\overline{u'w'}$, and (f) spanwise vorticity ω_y for the $Re_D = 18{,}600$ case.

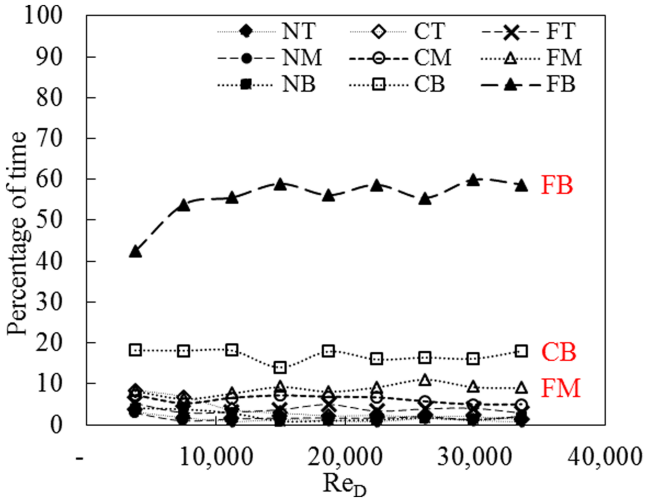

Figure 4. Percentage of time fish spent in each zone at different Re_D steps. Δ, □, and Δ markers indicate percentage time the fish spent in volume zones defined in Figure 1 where FB is the far bed volume, CB is the central bed volume, and FM is the far middle-depth volume.

in Figure 3. The percentage of time spent in each zone increased with increasing L_u/L_{fish}, indicating that the fish preferred zones where the turbulent length scale was much less than half their length. When $L_u/L_{fish} \geq 0.4$, the percentage of time starts to decrease, as fish begin to avoid zones where the turbulent length scale approached 50% of the fish length (Figure 6a). Fish could station hold in zones of low turbulence intensity, with a preference for the range $0.3 < TI_u < 0.4$, a preference that was less evident with increasing TI_u. For all Re_D steps, percentage time decreased with increasing turbulence intensity (TI_u) as fish spent less time in zones of higher TI_u (GLMM, d.f.1, $p < 0.001$).

3.2.2. Distribution of Spill Occurrences Over the Test Area

For all 28 fish tested, 317 spills were recorded in total and distributed in the flow volume zones as depicted in Figure 5b. The number of spills per fish was dependent on fish length and weight, since larger fish spilled less than small fish (GLMM, d.f.1, $p = 0.033$). Higher values of turbulence integral length scale to standard fish length ratio (L_u/L_{fish}) corresponded to higher numbers of spills (Figure 6a). Spanwise vortices with a length scale range of $0 \leq L_u/L_{fish} \leq 0.55$ were present in the cylinder wake, and spills were observed across the whole range, with the number of spills generally increasing with L_u/L_{fish} ratio and the maximum spills occurring toward the upper limit of the range where $L_u/L_{fish} = 0.55$ (Figure 6a). Similarly, high numbers of spills were recorded in the near wake zones of highest vertical Reynolds shear stress $\langle \tau_{uw} \rangle$, and vorticity $\langle \omega_y \rangle$ (Figures 4b and 4c). The number of spills gradually increased with increasing Re_D, reaching a maximum at $Re_D = 14{,}930$ ($U_0 = 30$ cm/s) and decreased slightly for the remaining Re_D steps (Figure 6). For $U_0 < 30$ cm/s, the number of spills increased with each velocity step and was found to correlate with increasing cross-sectionally averaged velocity per volume zone (GLMM, d.f.1, $p < 0.001$), and the higher the amount of time the fish spent in the zone, the higher the likelihood of spills occurring, which is evident in the FB and central bed zones (GLMM, d.f.1, $p < 0.001$; Figure 7). For $U_0 > 30$ cm/s, the number of spills significantly depended on the velocity step U_0 (GLMM, d.f.1, $p = 0.004$), the ratio of velocity/fish length (body-length per second, based on fish total length; GLMM, d.f.1, $p = 0.005$), the fish's momentum (fish mass * $\overline{u}$; GLMM, d.f.1, $p = 0.031$), as well as the downstream distance from the cylinder (GLMM, d.f.1, $p < 0.001$; not shown here). The distribution of spills became less predictable at U_0 steps >30 cm/s as opposed to the near linear relationship of the number of spills with Re_D for $U_0 < 30$ cm/s ($R^2 = 0.993$; Figure 7). Therefore, occurrence of spills depended on the fish's length and weight and was significantly affected by the Re_D, the Reynolds stresses and the vorticity (Figures 6b and 6c).

3.2.3. Frequency of Spill Events Over the Step Velocity Test

Zones furthest from the cylinder, where the wake turbulence intensities had decayed, were the preferred fish refuge due to the reduced likelihood of spills occurring (Figure 5c). The frequency of spills (spills per min) decreased with increasing downstream distance from the cylinder (GLMM, d.f.1, $p < 0.001$). The near wake zones, where the fish spent the least amount of time, featured the highest spill frequency. The proportion of time that fish spent in each zone increased with increasing downstream distance from the cylinder and increased with proximity to the bed (Figure 5a). Overall, the highest percentage of spills occurred in the

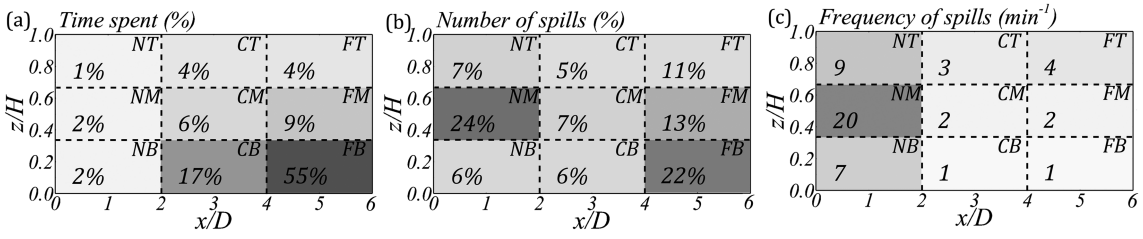

Figure 5. Distributions of percentage of (a) time spent, (b) spills, and (c) spill frequency (min^{-1}) in each flow volume zone (outlined in Figure 1). The zones with the highest proportion of time, spills, and frequency of spills are shaded in gray.

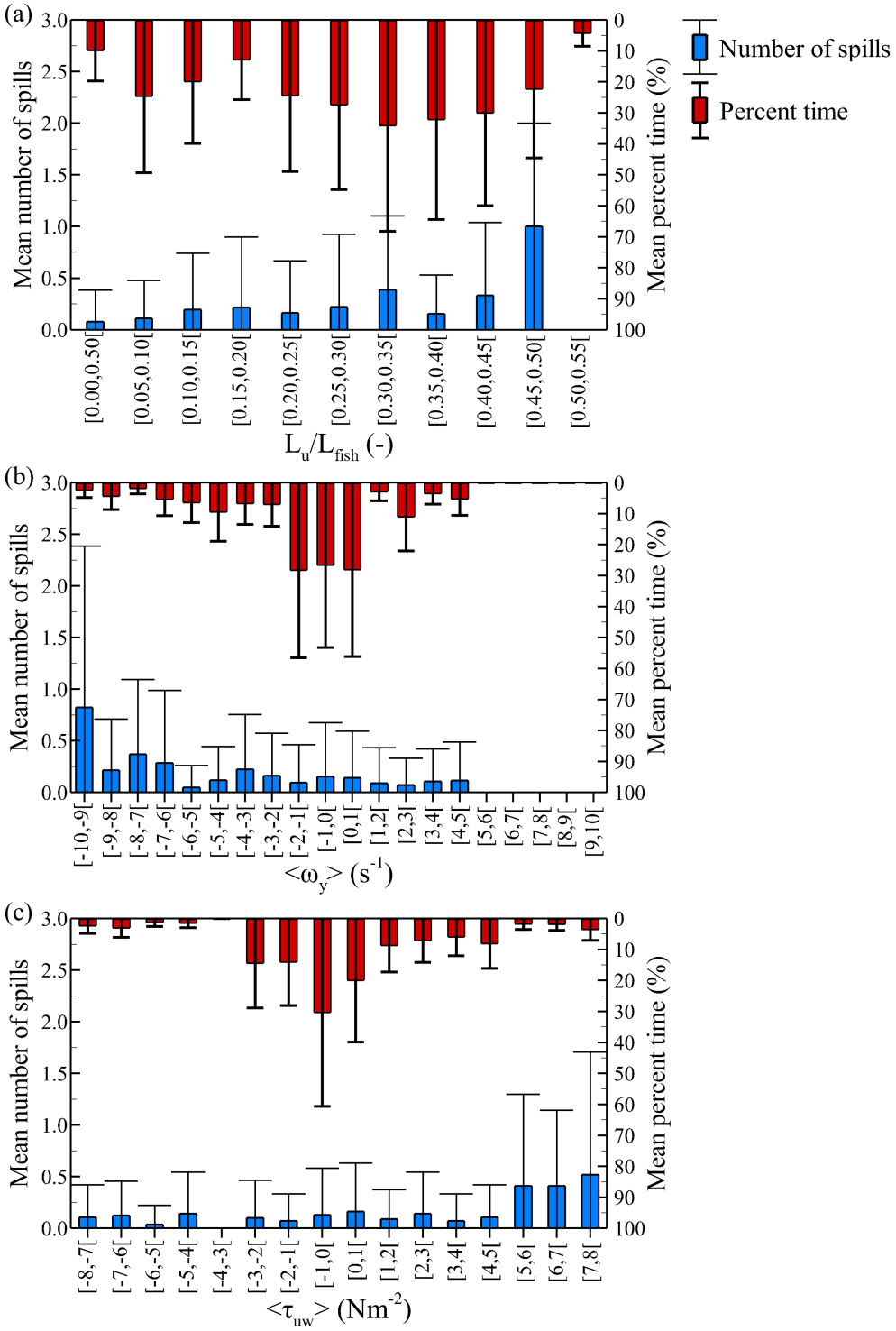

Figure 6. Mean number of spills and mean proportion of time (%) the fish spent (mean ± *SD*) relative to the flow characteristics of (a) the ratio of turbulence length scale over fish length L_u/L_{fish} in 0.05 intervals, (b), zone averaged *y*-vorticity component $\langle\omega_y\rangle$ in 1-s^{-1} intervals, and (c) vertical Reynolds shear stress τ_{uw} in 1 Nm^{-2} intervals. Error bars represent the standard deviation.

far wake, followed by the near wake and the center wake. The flow zones with the most spills were NM (24%) and FB (22%). In the NM zone, in particular, fish spilled the most but spent the least amount of time here, so they spilled almost immediately after swimming into this area and therefore tended to avoid this area. The

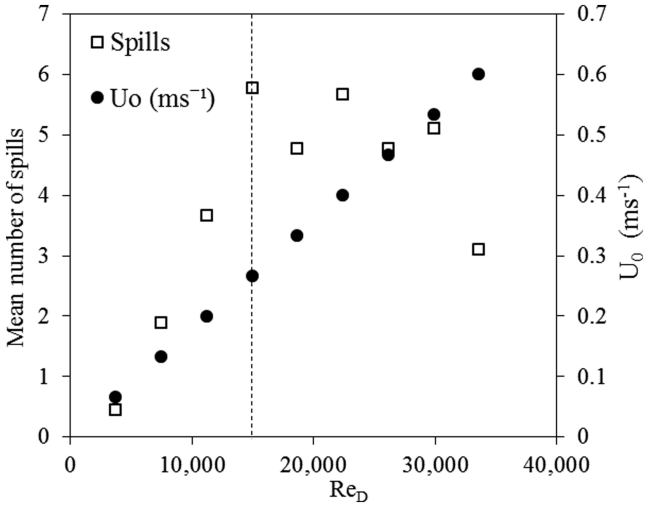

Figure 7. Mean number of spills relative to the cylinder Reynolds number and the cross-sectionally averaged velocity U_0 (ms^{-1}). The dashed line indicates the $Re_D = 14{,}930$ ($U_0 = 0.3$ ms^{-1}) after which the number of spills remains relatively constant, before decreasing at the last velocity step.

FB zone was the preferred station holding zone for the fish as they spent over half their time there, resulting in a proportionately high number of spills but the lowest frequency of spills (Figure 8).

The frequency of spills significantly varied with Re_D (Figure 8) and vorticity (GLMM, d.f.1, $p < 0.05$) and was significantly dependent on the fish's length ($p < 0.001$), as well as the momentum of the fish (mass * $\overline{u}$; GLMM, d.f.1, $p < 0.001$). Furthermore, the frequency of spills increased with increasing ratio of turbulence length scale to cylinder diameter (L_u/D; data not shown) but increased with decreasing L_u/L_{fish} (GLMM, d.f.1, $p < 0.05$). Zones of higher τ_{uw} also showed increased frequency of spills ($p < 0.001$). Furthermore, the highest spatial variation of vorticity was in the NB and NM zones, with the remaining zones showing lesser standard deviation, highlighting the predominance of negative vorticity (clockwise eddies) in the NM zone, since only the NB zone contained positive vorticity (counterclockwise rollers; Figure 9). This considerably affected the frequency of spills, which was highest in the NM and NB zones where vorticity standard deviation was greater than 2.78 (more than 60% of the cross-sectionally averaged vorticity; Figure 10). This result suggests that the near wake had less predictable flows due to the higher flow unsteadiness, leading to the lower preference of the fish to station hold in these zones and to the higher frequencies of spills observed.

The near wake, where highest fluctuations of vorticity above the mean were present (Figure 9), was characterized by the highest spill frequencies (Figure 10), suggesting that these flows were significantly unpredictable for the fish compared to the other zones. These near wake zones also had the highest instances of τ_{uv}, and τ_{uw} from the shear layer breakdown from the cylinder. The horizontal orientation of the cylinder considered in this study created a vortex shedding regime in which the momentum exchange was most dominant in the vertical direction, that is, *XZ* plane, with mean$|\tau_{uv}| \leq 1.5$ Nm^{-2} and$|\tau_{uw}| \leq 8$ Nm^{-2} (|indicate absolute value), making Reynolds shear stress in the *XZ* plane (normal to the cylinder's axes) over five times stronger than those in the *XY* (horizontal) plane. Due to the ground proximity that rendered the wake vortex shedding assymetric, the NM zone, where rollers were clockwise (negative) and τ_{uw} was downwards (positive), was among the least frequented zones, yet showed the highest number of spills and twice the frequency of spills of any other zone. In contrast, the NB zone of the lower shear layer was similarly frequented (Figure 5a) and had similar magnitude of Reynolds shear stresses and vorticity, but these were negative, that is, opposite to those in the upper shear layer of NM due to the different vertical momentum exchange direction (Figure 3). As a result, the NB zone showed significantly lower numbers of spills as well as a lower frequency of spills than the NM zone, which suggests that it is important whether positive or negative turbulent shear stresses and clockwise or counterclockwise eddy vortices are acting on the fish, influencing the swimming stability of fish. A summary figure that illustrates the interactions of the fish and the spanwise vortex dynamics as well as the distribution of forces acting on the fish is given in Figure 11.

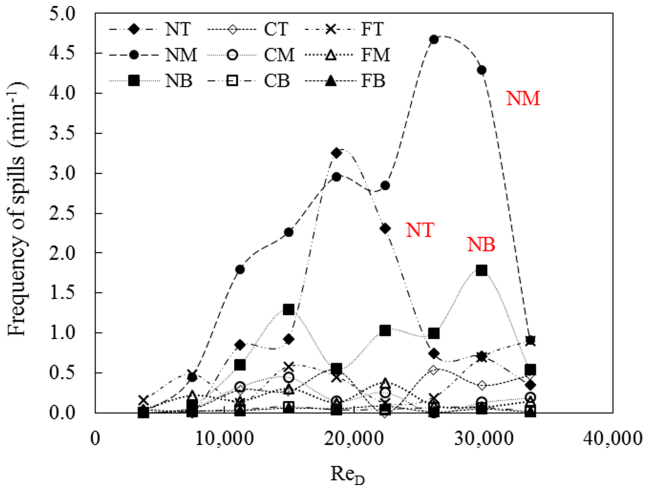

Figure 8. Variation of frequency of spills (min^{-1}) per Re_D and flow volume zones shows that the near wake zones (NB, NM, NT) had the highest ratio of spill occurrence over amount of time the fish spent in the zone, and this frequency changed with increasing Re_D. The center and far wake zones (CB, CM, CT, FB, FM, FT) where fish preferred to station hold show little to no variation in frequency of spills over the range of Re_D.

4. Discussion

The swimming stability and habitat usage of Nile tilapia fish in the turbulent wake of a horizontal cylinder were investigated to evaluate fish interaction with turbulence characteristics under Reynolds numbers (Re_D) ranging from 3,730 to 33,590. Fish habitat preference was significantly influenced by local velocity, turbulence intensity, turbulent kinetic energy, turbulence integral length scale, vorticity, and Reynolds shear stresses. For all Re_D steps, fish spent less time in zones of higher turbulence intensity, to

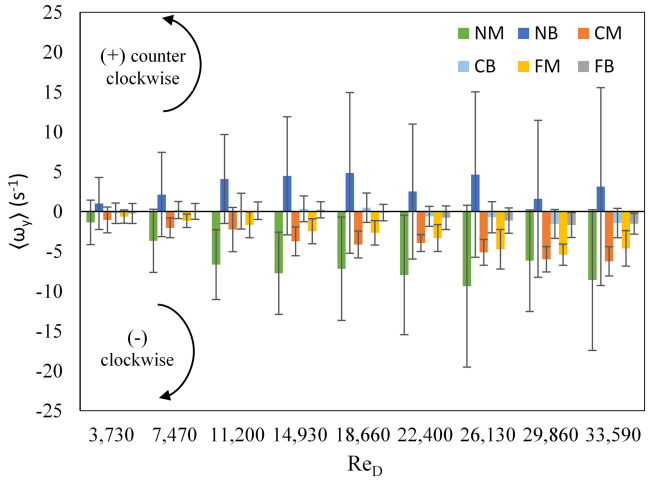

Figure 9. Zone-averaged vorticity $\langle\omega_y\rangle$ (mean ± *SD*) distribution by flow volume zones for each Re_D. Positive vorticity indicates vortices rotating counterclockwise, while negative values denote eddies rotating clockwise. Flow volume zones are outlined in Figure 1. Error bars represent the standard deviation.

avoid the high swimming costs associated with elevated turbulence intensities (Enders et al., 2003; Hockley et al., 2014; Odeh et al., 2002; Pavlov et al., 2000). The change in spill occurrence after the intermediate Re_D of 14,930 (Figure 7) is perhaps due to changes in the shape of eddies as turbulent shedding regimes vary with Re_D. In addition, Nile tilapia do respond positively to behavioural conditioning (Mesquita & Young, 2007) and therefore could have adjusted their spill responses through learned behavior in the step velocity test, similar to behaviours of adjustment to turbulence observed by Maia et al. (2015). Fish were assumed to be within the critical swimming capabilities (Alsop et al., 1999), and showed no signs of fatigue in the swimming observations.

Although other researchers have found that habitat preference varies with flow cross-sectional averaged velocity (Pavlov et al., 2000; Enders et al., 2003; Tritico & Cotel, 2010), here, the percentage of time spent in each zone did not vary significantly with increasing Re_D, as also reported by Maia et al. (2015). This could be attributed to the relatively similar distribution of velocities and turbulence in all zones throughout the step test and the FB zone remained the preferred region due to the lower magnitues of τ_{uw}, τ_{uv}, and ω_y. Furthermore, the threshold for the distribution of habitat choice and occurance of spills of L_u/L_{fish} being 50% (Figure 6a) supports the idea of there being an ideal ratio of turbulence length scale to fish length as fish are predicted to prefer turbulent length scales that are either much smaller or much greater than their body length (Lupandin, 2005; Odeh et al., 2002; Pavlov et al., 2000; Tritico & Cotel, 2010; Wang et al., 2016; Webb & Cotel, 2011). This is also in keeping with the turbulence length scale to fish length ratio threshold of 0.66 reported by Pavlov et al. (2000) and Lupandin (2005), although small variations of this threshold might be due to interspecies differences, individual fish shape and hydrodynamic measurements techniques and calculations of turbulent length scale (Lacey et al., 2012; Liao, 2007). Similar to other studies, the high preference for zones furthest from the cylinder was due to the presence of lowest vorticity, Reynolds shear stresses (Hockley et al., 2014; Silva, Katopodis, et al., 2012; Silva, Santos, et al., 2012) and turbulent kinetic energy (Smith et al., 2006).

Tritico and Cotel (2010) demonstrated that the axis of rotation of the dominating vortices, vertical axis for vertical cylinders, and spanwise axis for horizontal spanwise cylinders yields different effects on swimming stability as spanwise rollers resulted in more spills than vertical rollers, for eddies over 75% of the fish length. The Kármán gaiting swimming behavior described by Liao et al. (2003) was not observed in the current study, as fish were unable to take advantage of the von Kármán street typically composed of vertical rollers, which are not present in horizontal cylinder flow. This is because the eddy's plane of orientation (*XZ* plane) is perpendicular to the fish's spine and axis of undulation, which is employed in swimming, along with fin oscillations to propel longitudinally and produce lateral movements of their body (*XY* plane) (Lauder & Madden, 2007; Pavlov et al., 2000; Webb, 2002, 2004), and hence, the main eddy torque and vorticity work against the fish by dominating the vertical (*XZ*) plane where motor control is most limited. This proposed reasoning is shown in Figure 11.

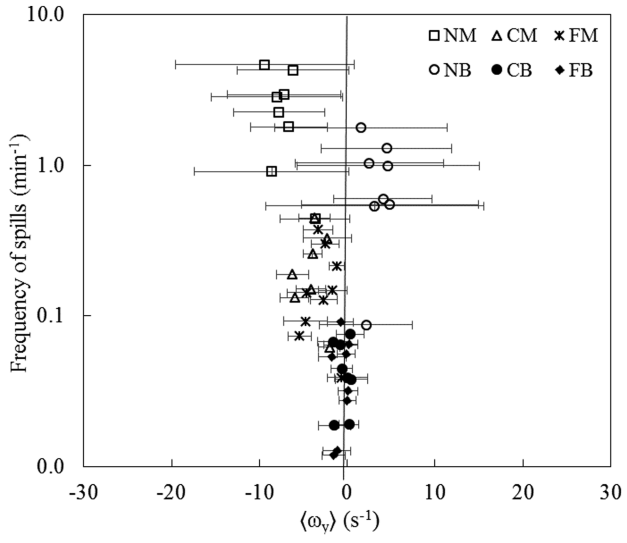

Figure 10. Semi-log plot of average frequency of spills relative to the zone averaged *y*-vorticity $\langle\omega_y\rangle$ (mean ± *SD*).

Reynolds shear stresses are of substantial physical importance in the fish's environment as they indicate the magnitude and distribution of turbulent momentum exchange, yet often omitted in fish swimming behavior studies (Lacey et al., 2012). In fish pass studies, Reynolds shear stresses are the most significant flow characteristic influencing transit time and successful passage, particularly for small fish (Silva et al., 2011; Silva, Katopodis, et al., 2012; Silva, Santos, et al., 2012). Even though the Reynolds shear stress values of the current experiment are lower than those in rivers (Lacey et al., 2012), current results clearly show that it is important to consider Reynolds shear stresses in fish-turbulence

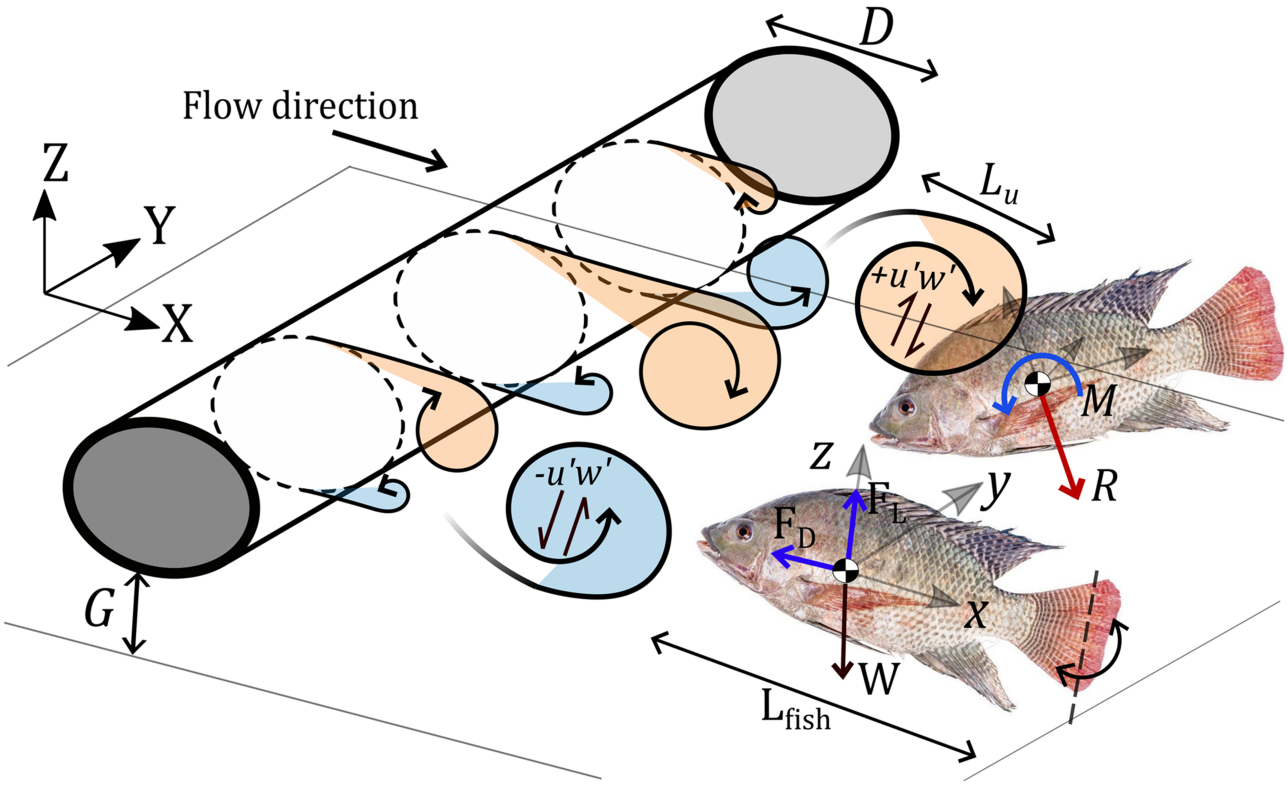

Figure 11. Schematic of the interaction between the alternating vortex shedding developed behind the horizontal cylinder and the fish including the force balance, where F_D is drag force, F_L is lift force, W is fish's weight, L_u is the length scale of a given vortex, L_{fish} is the fish's length, and R and M are the force vector and resulting moment, which cause a turning reaction when the fish becomes unbalanced, and $u'w'$ illustrates the Reynolds shear stress.

interaction studies (Figure 11). The balance of hydrodynamic forces and the resultant torques and moments acting on the fish challenge its ability to maintain posture and swim unimpeded (Cotel et al., 2006; Drucker & Lauder, 1999; Liao, 2007; Lupandin, 2005; Odeh et al., 2002; Pavlov et al., 2000; Silva, Katopodis, et al., 2012; Silva, Santos, et al., 2012; Tritico & Cotel, 2010; Wang & Chanson, 2018; Webb, 2002; Webb & Cotel, 2010). However, considering the orientation plane of vortices and magnitude of hydrodynamic forces requires the inclusion of their direction, which this study has demonstrated to be essential.

The balance of hydrodynamic forces surrounding a swimming fish are intricate; the fish uses coordinated propulsive maneuvers to overcome spanwise hydrodynamic forces (F_D), uplift forces (F_L) from the fluid dynamics and to compensate against its weight (W) as well as vertical or horizontal Reynolds shear stresses dependent on an obstacle's orientation (Figure 11). The unbalanced resultant forces create overturning moments that affect the fish's locomotion (Drucker & Lauder, 1999, 2000; Nauen & Lauder, 2002; Webb, 2002). Therefore, distribution, intensity, and direction of hydrodynamic forces exerted on the fish will aid propulsion or hinder swimming kinematics; whether the force is toward or counter to the fish works for or against the fish's propulsive maneuvers. The interdependence of vorticity and Reynolds shear stresses cannot be neglected, and as our results suggest, downward Reynolds shear stresses, and rollers with clockwise rotation destabilize the fish more often than those of similar extent but opposite sign, that is, upward direction (Figure 9).

Fish swimming kinematic studies might benefit from more emphasis on Reynolds stresses to better explain fish size-dependent responses to turbulent flows. The locomotion of smaller fish likely becomes overwhelmed by resultant turbulent stresses that exceed their capablility for stabilization manouvers, leading to more frequent losses of stability than their larger counterparts (Cada & Odeh, 2001; Lupandin, 2005; Pavlov et al., 2000; Webb, 2002). Variations of fish behavior in turbulent flows due to individual physiological differences, in addition to size, life stage, and species (e.g., Pavlov et al., 2000; Plew et al., 2007), could become clearer by specifiying whether local Reynolds shear stresses and vorticity are positive or negative, that is,

considering the directionality of the momentum exchange and velocity gradients, in the characterization of the hydrodynamics in environmental turbulent flows.

5. Conclusions

In summary, in order to evaluate the turbulence metrics that govern fish swimming behavior, swimming kinematics and habitat preference of fish were investigated in the turbulent wake of a horizontal cylinder where the dominant plane of vortex shedding was the *XZ* plane. Habitat preference was determined by the turbulence intensity, turbulent kinetic energy, vorticity, Reynolds shear stress, and turbulent length scale relative to fish length as fish avoided areas of relatively high turbulence. Similarly, these parameters influenced the occurrence of spills in addition to the Reynolds number, and fish size and weight, with smaller fish being more perturbed than larger ones. The number of spills generally increased with L_u/L_{fish} ratio with the maximum spills occurring toward the upper limit where the eddy length was 45% to 50% of the fish length. The highest rate of spills occurred in the zones where the upper shear layer had highest magnitudes of negative (downward-acting) Reynolds shear stresses and negative vorticity (clockwise rotating vortices). Overall, spanwise rollers yield different effects on swimming stability compared to the vertical vortices found in vertical cylinder wakes, as the main eddy torque and vorticity work against the fish by dominating the plane where motor control is most limited.

Therefore, in addition to the size of eddies, the plane of dominant eddy rotation, and the magnitude of Reynolds shear stresses, we highlight that the direction of eddy rotation and that of vertical turbulent momentum exchange are physical flow characteristics that impact fish swimming kinematics. These results further our understanding of fish swimming behavior and can inform design and refinement of fish-friendly structures including fish passes, hydropower turbines, and restorations of fluvial environments. In fish passes and altered environments, the prevention of flow dominated by spanwise rollers and downward turbulent shear stresses could benefit fish movement and passage, while usage of spanwise rollers downstream of hydropower schemes (e.g., Archmedis screw turbines) could benefit fish guidance efforts to deter fish from turbine blades and perilous flows.

Acknowledgments
We thank Amy Ellison for providing fish care, Rhiannon Hunt for statistical advice, and two anonymous reviewers for their comments on an earlier version of this manuscript. Data are available via https://doi.org/10.5281/zenodo.3471636 (Muhawenimana et al., 2019).

References

Alsop, D. H., Kieffer, J. D., & Wood, C. M. (1999). The effects of temperature and swimming speed on instantaneous fuel use and nitrogenous waste excretion of the Nile tilapia. *Physiological and Biochemical Zoology*, *72*(4), 474–483. https://doi.org/10.1086/316686

Bates, D., Mächler, M., Bolker, B., & Walker, S. (2015). Fitting linear mixed-effects models using lme4. *Journal of Statistical Software*, *67*(1), 1–48. https://doi.org/10.18637/jss.v067.i01

Cada, G. F., & Odeh, M. (2001). *Turbulence at Hydroelectric Power Plants and its Potential Effects on Fish*, *Report to Bonneville Power Administration*, (). Portland, Oregon: Bonneville Power Administration (BPA). https://doi.org/10.2172/781814

Cotel, A. J., Webb, P. W., & Tritico, H. (2006). Do brown trout choose locations with reduced turbulence? *Transactions of the American Fisheries Society*, *135*(3), 610–619. https://doi.org/10.1577/T04-196.1

Crowder, D. W., & Diplas, P. (2002). Vorticity and circulation: Spatial metrics for evaluating flow complexity in stream habitats. *Canadian Journal of Fisheries and Aquatic Sciences*, *59*(4), 633–645. https://doi.org/10.1139/f02-037

Douglas, J. F., Gasiorek, J., Swaffield, J., & Jack, L. (2011). *Fluid Mechanics (sixth)*. Harlow: Pearson Education.

Drucker, E. G., & Lauder, G. V. (1999). Locomotor forces on a swimming fish: Three-dimensional vortex wake dynamics quantified using digital particle image velocimetry. *The Journal of Experimental Biology*, *202*(18), 2393–2412.

Drucker, E. G., & Lauder, G. V. (2000). A hydrodynamic analysis of fish swimming speed: wake structure and locomotor force in slow and fast labriform swimmers. *Journal of Experimental Biology*, *203*(16), 2379–2393.

Enders, E. C., Boisclair, D., & Roy, A. G. (2003). The effect of turbulence on the cost of swimming for juvenile Atlantic salmon (*Salmo salar*). *Canadian Journal of Fisheries and Aquatic Sciences*, *60*(9), 1149–1160. https://doi.org/10.1139/f03-101

Fuller, M. R., Doyle, M. W., & Strayer, D. L. (2015). Causes and consequences of habitat fragmentation in river networks. *Annals of the New York Academy of Sciences*, *1355*(1), 31–51. https://doi.org/10.1111/nyas.12853

Goring, D. G., & Nikora, V. I. (2002). Despiking acoustic Doppler velocimeter data. *Journal of Hydraulic Engineering*, *128*(1), 117–126. https://doi.org/10.1061/(ASCE)0733-9429(2002)128:1(117)

Graf, W. H., & Yulistiyanto, B. (1998). Experiments on flow around a cylinder; the velocity and vorticity fields. *Journal of Hydraulic Research*, *36*(4), 637–654. https://doi.org/10.1080/00221689809498613

Hockley, F. A., Wilson, C. A. M. E., Brew, A., & Cable, J. (2014). Fish responses to flow velocity and turbulence in relation to size, sex and parasite load. *Journal of the Royal Society, Interface/the Royal Society*, *11*(91), 20130814. https://doi.org/10.1098/rsif.2013.0814

Jamieson, E. C., Rennie, C. D., & Townsend, R. D. (2013). Turbulence and vorticity in a laboratory channel bend at equilibrium clear-water scour with and without stream barbs. *Journal of Hydraulic Engineering*, *139*(3), 259–268. https://doi.org/10.1061/(ASCE)HY.1943-7900.0000673

Jesson, M., Sterling, M., & Bridgeman, J. (2013). Despiking velocity time-series—Optimisation through the combination of spike detection and replacement methods. *Flow Measurement and Instrumentation*, *30*, 45–51. https://doi.org/10.1016/j.flowmeasinst.2013.01.007

Katopodis, C., & Williams, J. G. (2012). The development of fish passage research in a historical context. *Ecological Engineering*, *48*, 8–18. https://doi.org/10.1016/j.ecoleng.2011.07.004

Lacey, R. W. J., Neary, V. S., Liao, J. C., Enders, E. C., & Tritico, H. M. (2012). The IPOS framework: Linking fish swimming performance in altered flows from laboratory experiments to rivers. *River Research and Applications*, *28*(4), 429–443. https://doi.org/10.1002/rra.1584
Larinier, M. (2001). Environmental issues, dams and fish migration. FAO Fisheries Technical Paper (Vol. 419)
Lauder, G. V., & Madden, P. G. A. (2007). Fish locomotion: Kinematics and hydrodynamics of flexible foil-like fins. *Experiments in Fluids*, *43*(5), 641–653. https://doi.org/10.1007/s00348-007-0357-4
Lehmkuhl, O., Rodríguez, I., Borrell, R., & Oliva, A. (2013). Low-frequency unsteadiness in the vortex formation region of a circular cylinder. *Physics of Fluids*, *25*(8), 085109. https://doi.org/10.1063/1.4818641
Leng, X., & Chanson, H. (2017). Unsteady velocity profiling in bores and positive surges. *Flow Measurement and Instrumentation*, *54*, 136–145.
Liao, J. C. (2007). A review of fish swimming mechanics and behavior in altered flows. *Philosophical Transactions of the Royal Society, B: Biological Sciences*, *362*(1487), 1973–1993. https://doi.org/10.1098/rstb.2007.2082
Liao, J. C., Beal, D. N., Lauder, G. V., & Triantafyllou, M. S. (2003). The Kármán gait: Novel body kinematics of rainbow trout swimming in a vortex street. *Journal of Experimental Biology*, *206*(6), 1059–1073. https://doi.org/10.1242/jeb.00209
Lupandin, A. I. (2005). Effect of flow turbulence on swimming speed of fish. *Biology Bulletin*, *32*(5), 461–466. https://doi.org/10.1007/s10525-005-0125-z
Maia, A., Sheltzer, A. P., & Tytell, E. D. (2015). Streamwise vortices destabilize swimming bluegill sunfish (*Lepomis macrochirus*). *Journal of Experimental Biology*, *218*(5), 786–792. https://doi.org/10.1242/jeb.114363
Mesquita, F. d. O., & Young, R. J. (2007). The behavioural responses of Nile tilapia (*Oreochromis niloticus*) to anti-predator training. *Applied Animal Behavior Science*, *106*, 144–154. https://doi.org/10.1016/j.applanim.2006.06.013
Muhawenimana, V., Wilson, A. M. E. C., Ouro, P., and Cable, J. (2019). *Spanwise cylinder wake hydrodynamics and fish behavior: Data*. https://doi.org/10.5281/ZENODO.3471637
Murchie, K. J., Hair, K. P. E., Pullen, C. E., RedPath, T. D., Stephens, H. R., & Cooke, S. J. (2008). Fish response to modified flow regimes in regulated rivers: Research methods, effects and opportunities. *River Research and Applications*, *24*, 197–217. https://doi.org/10.1002/rra.1058
Nauen, J. C., & Lauder, G. V. (2002). Quantification of the wake of rainbow trout (*Oncorhynchus mykiss*) using three-dimensional stereoscopic digital particle image velocimetry. *The Journal of Experimental Biology*, *205*(21), 3271–3279.
Nikora, V., Aberle, J., & Biggs, B. (2003). Effects of fish size, time to fatigue and turbulence on swimming performance: A case study of *Galaxias Maculatus*. *Journal of Fish Biology*, *63*, 1365–1382. https://doi.org/10.1046/J.1095-8649.2003.00241.X
Noonan, M. J., Grant, J. W. A., & Jackson, C. D. (2012). A quantitative assessment of fish passage efficiency. *Fish and Fisheries*, *13*(4), 450–464. https://doi.org/10.1111/j.1467-2979.2011.00445.x
Nortek, A. S. (2009). *Vectrino Velocimeter User Guide*. Norway: Vangkroken.
Odeh, M., Noreika, J. F., Haro, A., Maynard, A., Castro-Santos, T., & Cada, G. F. (2002). Evaluation of the effects of turbulence on the behavior of migratory fish, Final Report 2002.
Oner, A. A., Salih Kirkgoz, M., & Sami Akoz, M. (2008). Interaction of a current with a circular cylinder near a rigid bed. *Ocean Engineering*, *35*(14–15), 1492–1504. https://doi.org/10.1016/j.oceaneng.2008.06.005
Pavlov, D. S., Lupandin, A. I., & Skorobogatov, M. A. (2000). The effects of flow turbulence on the behavior and distribution of fish. *Journal of Ichthyology*, *40*(2), 232–261.
Plew, D. R., Nikora, V. I., Larned, S. T., Sykes, J. R. E., & Cooper, G. G. (2007). Fish swimming speed variability at constant flow: *Galaxias maculatus*. *New Zealand Journal of Marine and Freshwater Research*, *41*(2), 185–195. https://doi.org/10.1080/00288330709509907
Pope, S. B. (2000). *Turbulent Flows*. Cambridge: Cambridge University Press. https://doi.org/10.1017/CBO9780511840531
Price, S. J., Sumner, D., Smith, J. G., Leong, K., & Paidoussis, M. P. (2002). Flow visualization around a circular cylinder near to a plane wall. *Journal of Fluids and Structures*, *16*(2), 175–191. https://doi.org/10.1006/jfls.2001.0413
Sarkar, S., & Sarkar, S. (2010). Vortex dynamics of a cylinder wake in proximity to a wall. *Journal of Fluids and Structures*, *26*(1), 19–40. https://doi.org/10.1016/j.jfluidstructs.2009.08.003
Silva, A. T., Katopodis, C., Santos, J. M., Ferreira, M. T., & Pinheiro, A. N. (2012). Cyprinid swimming behavior in response to turbulent flow. *Ecological Engineering*, *44*, 314–328. https://doi.org/10.1016/j.ecoleng.2012.04.015
Silva, A. T., Santos, J. M., Ferreira, M. T., Pinheiro, A. N., & Katopodis, C. (2011). Effects of water velocity and turbulence on the behavior of Iberian barbel (*Luciobarbus bocagei*, Steindachner 1864) in an experimental pool-type fishway. *River Research and Applications*, *27*(3), 360–373. https://doi.org/10.1002/rra.1363
Silva, A. T., Santos, J. M., Ferreira, M. T., Pinheiro, A. N., & Katopodis, C. (2012). Passage efficiency of offset and straight orifices for upstream movements of Iberian barbel in a pool-type fishway. *River Research and Applications*, *28*(5), 529–542. https://doi.org/10.1002/rra.1465
Smith, D. L., Brannon, E. L., Shafii, B., & Odeh, M. (2006). Use of the average and fluctuating velocity components for estimation of volitional rainbow trout density. *Transactions of the American Fisheries Society*, *135*(2), 431–441. https://doi.org/10.1577/T04-193.1
Team, R. C. (2018). *R: A Language and Environment for Statistical Computing*. Austria: R Foundation for Statistical Computing.
Team, R. (2016). *RStudio: Integrated Development for R*. Boston: RStudio Inc.
Tritico, H. M., & Cotel, A. J. (2010). The effects of turbulent eddies on the stability and critical swimming speed of creek chub (*Semotilus atromaculatus*). *Journal of Experimental Biology*, *213*(13), 2284–2293. https://doi.org/10.1242/jeb.041806
Wahl, T. L. (2003). Discussion of "despiking acoustic Doppler velocimeter data" by Derek G. Goring and Vladimir I. Nikora. *Journal of Hydraulic Engineering*, *129*(6), 484–487. https://doi.org/10.1061/(ASCE)0733-9429(2003)129:6(484)
Wang, H., & Chanson, H. (2018). Modelling upstream fish passage in standard box culverts: Interplay between turbulence, fish kinematics, and energetics. *River Research and Applications*, *34*(3), 244–252. https://doi.org/10.1002/rra.3245
Wang, H., Chanson, H., Kern, P., & Franklin, C. (2016). Culvert hydrodynamics to enhance upstream fish passage: Fish response to turbulence. In *Proceedings of 20th Australasian Fluid Mechanics Conference*, *Australasian Fluid Mechanics Society*, (pp. 1–4). Australia: Perth WA.
Wang, R. W., David, L., & Larinier, M. (2010). Contribution of experimental fluid mechanics to the design of vertical slot fish passes. *Knowledge and Management of Aquatic Ecosystems*, *396*, 1–21. https://doi.org/10.1051/kmae/2010002
Webb, P. W. (1998). Entrainment by river chub nocomis micropogon and smallmouth bass *Micropterus dolomieu* on cylinders. *The Journal of Experimental Biology*, *201*(16), 2403–2412.
Webb, P. W. (2002). Control of posture, depth, and swimming trajectories of fishes. *Integrative and Comparative Biology*, *42*(1), 94–101. https://doi.org/10.1093/icb/42.1.94
Webb, P. W. (2004). Response latencies to postural disturbances in three species of teleostean fishes. *Journal of Experimental Biology*, *207*(6), 955–961. https://doi.org/10.1242/jeb.00854

Webb, P. W., & Cotel, A. J. (2010). Turbulence: Does vorticity affect the structure and shape of body and fin propulsors? *Integrative and Comparative Biology*, *50*(6), 1155–1166. https://doi.org/10.1093/icb/icq020

Webb, P. W., & Cotel, A. J. (2011). Assessing possible effects of fish-culture systems on fish swimming: The role of stability in turbulent flows. *Fish Physiology and Biochemistry*, *37*(2), 297–305. https://doi.org/10.1007/s10695-011-9497-9

Williams, J. G., Armstrong, G., Katopodis, C., Larinier, M., & Travade, F. (2012). Thinking like a fish: A key ingredient for development of effective fish passage facilities at river obstructions. *River Research and Applications*, *28*(4), 407–417. https://doi.org/10.1002/rra.1551

Williamson, C. H. K. (1996). Vortex dynamics in the cylinder wake. *Annual Review of Fluid Mechanics*, *28*(1), 477–539.